New Results

Sterile kidney tissue injury induces neutrophil swarming in lung alveolar capillaries

Yohei Komaru[1], Liang Ning[1], Carine Lama[1], Anusha Suresh[1], Eirini Kefaloyianni[2], Mark J. Miller[4], Andreas Herrlich[1,3]*

Affiliations:

1. Division of Nephrology, Department of Medicine, Washington University School of Medicine, St. Louis, MO, USA
2. Division of Rheumatology, Department of Medicine, Washington University School of Medicine, St. Louis, MO, USA
3. VA Saint Louis Health Care System, John Cochran Division, St. Louis, MO, USA
4. Division of Infectious Diseases, Department of Medicine, Washington University School of Medicine, St. Louis, MO, USA

*Correspondence:

Andreas Herrlich, MD PhD

Division of Nephrology, Department of Medicine,
Washington University School of Medicine
660 South Euclid Avenue, St. Louis, MO 63110, USA
Email: aherrlich@wustl.edu

Abstract

Sterile tissue injury, such as by acute kidney injury, is common in the clinic and frequently associated with respiratory compromise and hypoxemia. We previously described signaling components released by the injured kidney that drive a remote inflammatory response in the lung. How this caused the resultant hypoxemia remained unclear. Here, we report that sterile kidney tissue injury induces rapid intravascular "neutrophil train" formation in lung capillaries, a novel form of neutrophil swarming. Rapid swarming is enhanced by decreased deformability of circulating neutrophils that impedes their lung capillary passage. Classical lung monocytes are required for neutrophil train formation and release CXCL2 to attract and retain stiffened neutrophils in lung capillaries which reduces capillary perfusion. We thus discovered a novel feature of kidney-lung crosstalk after sterile kidney tissue injury, capillary perfusion deficits that lead to reduced oxygenation despite proper alveolar function and ventilation, unlike in infectious inflammatory lung processes, such as bacterial pneumonia.

Introduction

Sterile organ tissue injury by cellular stress, ischemia or trauma can induce a systemic inflammatory syndrome and remote organ dysfunction (*1–4*). This organ crosstalk is driven by soluble circulating factors and neuronal signals, and frequently involves the induction of remote organ inflammation, which is emerging as a cause of clinically observed secondary organ complications and dysfunction in the kidney, lung, heart, or brain (*5–10*). Sterile tissue injury-induced remote lung inflammation with respiratory compromise has been reported in mice and humans after acute kidney injury (AKI) (*10–14*), after gut ischemia (*6*, *15*, *16*), or after surgical and other tissue trauma (*4*). We showed that ischemic acute kidney injury (AKI) induces rapid lung neutrophil accumulation detectable at 1 hour after AKI, peaking at 24 hours and coinciding with hypoxemia, and resolving only slowly over at least 1-2 weeks. Prevention of lung neutrophil accumulation also prevented hypoxemia (*14*). How sterile tissue injury initiates remote neutrophil accumulation with such speedy onset, what factors lead to their accumulation, and how remote lung neutrophil accumulation causes impaired oxygenation is not understood.

Here we show that sterile kidney tissue injury induces classical monocyte-dependent intravascular neutrophil "train" formation in lung alveolar capillaries, a novel form of intravascular neutrophil swarming that significantly impedes lung alveolar capillary blood flow. We identify initiating steps and signals that rapidly capture neutrophils in lung capillaries after kidney injury, and implicate classical monocyte released cytokines in their lung retention and assembly into neutrophil trains. Lung intravascular neutrophil swarming after sterile tissue injury may protect the organism from overt systemic action of neutrophils and inflammatory mediators, yet at the risk of hypoxemia due to reduced lung alveolar capillary perfusion and oxygen uptake.

Results

Single-cell transcriptomic landscape of remote lung inflammation induced by sterile kidney tissue injury

As an entry point to better understand cellular events involved in remote lung inflammation after sterile kidney tissue injury, we analyzed the transcriptomic landscape of lungs after ischemic acute kidney injury (AKI) at single-cell resolution. We scaled, standardized, and integrated single-cell RNA sequencing (scRNA-seq) data from mouse lungs 24 hours after sham surgery or after bilateral renal ischemia-reperfusion injury-induced AKI. After excluding doublets and cells with low-quality expression data, 31,787 lung cells underwent clustering using Seurat v4 (*17*). We identified 18 lung cell types using canonical marker genes as previously reported (*18*): 10 different immune cell types, alveolar epithelial cell type 1+2 (AT1+2), fibroblasts, pericytes, and 4 endothelial cell types (arterial, capillary, venous, lymphatic) (**Figure 1A**). Cell types and marker genes used for their identification were as follows: Neutrophils (*Retnlg*), B-cells (*CD79a*), T-cells (*Cd3d*), natural killer cells (*Gzma*), classical monocytes (*Plac8*$^+$, *Ly6c2* high), non-classical monocytes (*Plac8*$^+$, *Ly6c2* low), transitional monocytes (expressing both monocytes (*Plac8*) and interstitial macrophages (*C1qb*) markers), dendritic cells (*Cd209a*), alveolar macrophages (*Ear2*), AT1 (*Rtkn2*), AT2 cells (*Sftpd*), and fibroblasts (*Pdgfra*). Three separate endothelial cell clusters with high expression of *Eng* could be assigned to three different regions of the lung vasculature using *Hey1*, *Ednrb*, and *Vwf* as markers for arterial, capillary, and venous endothelial cells, respectively (*19*). Lymphatic endothelial cells were identified by high *Prox1* expression **(Figure 1B**). The lung cell types observed after AKI largely overlapped with those in the sham group; however, we identified several significant differences within the immune cell compartment, in particular in the neutrophil (small arrow) and monocyte/macrophage cluster (large arrowhead) (**Figure 1C**). The overall frequency of neutrophils and Ly6c$^+$ classical monocytes increased in the lung following AKI, with a trend of increase in transitional monocytes and interstitial macrophages, whereas the proportion of lymphocytes decreased compared to the sham condition (**Figure 1D**).

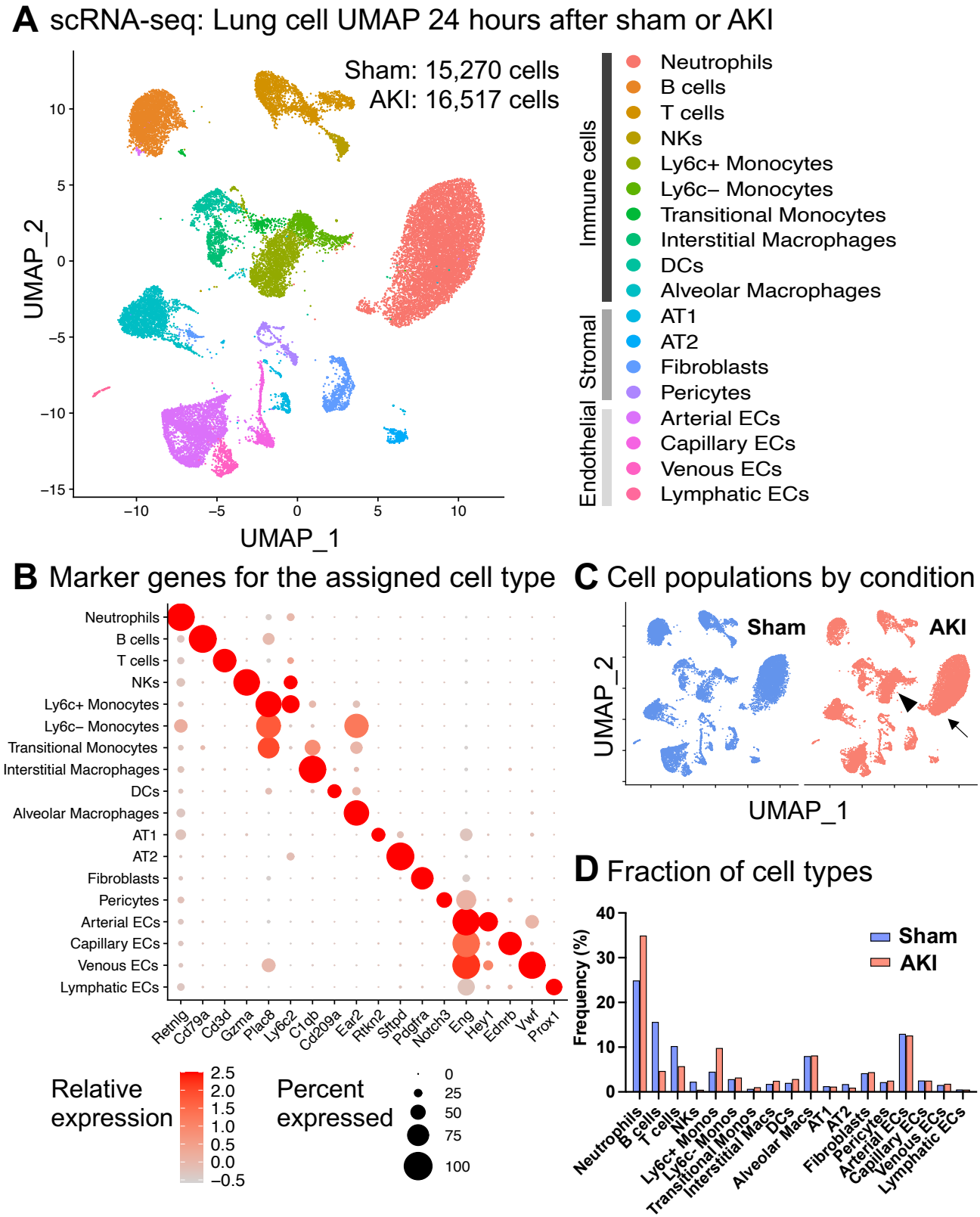

Fig. 1. Single-cell transcriptomic landscape of remote lung inflammation induced by ischemic acute kidney (tissue) injury (AKI).
(A) Uniform manifold approximation and projection (UMAP) representation of the lung cell dataset of 31,787 cells from four mice 24 hours after sham surgery (control) and four mice after 20-min bilateral kidney ischemia reperfusion injury, which causes acute kidney injury (AKI). Single-cell RNA sequencing analysis of sham and AKI combined identified 18 cell types within the lung. **(B)** Expression levels of the marker genes used for the

annotation of each cluster to a specific cell type. Dot size denotes percentage of cells expressing each gene and the color scale represents average gene expression levels. **(C)** The UMAP representation generated for lung cells from each experimental condition, sham or AKI. Two distinct cell populations, neutrophils and classical monocytes, undergo the most significant changes in AKI compared to sham (see arrows); also seen in cell quantification in 1D. **(D)** Quantification of the fraction of each cell type present in the lung after sham or AKI surgery. AKI: acute kidney injury; NK: natural killer cells; DCs: dendritic cells; AT1: type 1 pneumocytes; AT2: type 2 pneumocytes; EC: endothelial cells

Sterile kidney tissue injury induces lung accumulation of activated neutrophils and monocyte-derived interstitial macrophages

To examine changes in the neutrophil response after sterile kidney tissue injury, we extracted the neutrophil population, performed further clustering, and identified two distinct subtypes: Neutrophil 1 and Neutrophil 2 (**Figure 2A** UMAP), with the latter largely responsible for the threefold increase in total lung neutrophils after kidney injury compared to sham (**Figure 2A** graph). Using scRNA-seq data obtained at one time point, pseudotime analysis orders single-cell expression profiles based on their transcriptional similarity along a linear ruler, allowing to construct a developmental trajectory of cells. Pseudo-time trajectory analysis of our scRNA-seq dataset suggested that Neutrophil 2 emerged from Neutrophil 1 (**Figure 2B**). Analysis of differentially expressed genes (DEGs) showed that Neutrophil 1 featured genes associated with the basal neutrophil state, including *Ngp*, *Retnlg*, *Lyz2* and *Mmp8*, while Neutrophil 2 exhibited upregulated acute inflammatory genes such as *Nfkbia*, *Il1b*, *Cxcl2* and *Ccl4,* as seen in primed or activated neutrophils (**Figure 2C**). Gene ontology (GO) enrichment analysis conducted on upregulated DEGs comparing Neutrophil 2 vs Neutrophil 1 identified a predominance of genes associated with immune cell activation and chemotaxis in Neutrophil 2 (**Figure 2D**). Focusing on the expression of key inflammatory cytokines in our lung scRNA-seq dataset after ischemic kidney tissue injury, interleukin-1b (*Il1b*), interleukin-1 receptor type II (*Il1r2*), interleukin-17 receptor A (*Il17ra*), *Cxcl2*, and *Tnf* were most abundantly expressed within Neutrophil 2 (**Figure 2E**). Our monocyte analysis revealed that transitional monocytes express monocyte and macrophage markers, suggesting that they may be intermediate cells that are in the process of becoming lung interstitial macrophages. Pseudotime analysis showed that transitional monocytes emerge mainly from Ly6c^{+} classical monocytes (less from Ly6c^{-} non-classical monocytes) and develop into interstitial macrophages (**Figure 2F**). Thus, sterile kidney tissue injury leads to lung accumulation of primed and/or activated inflammatory neutrophils and of monocyte-derived interstitial macrophages.

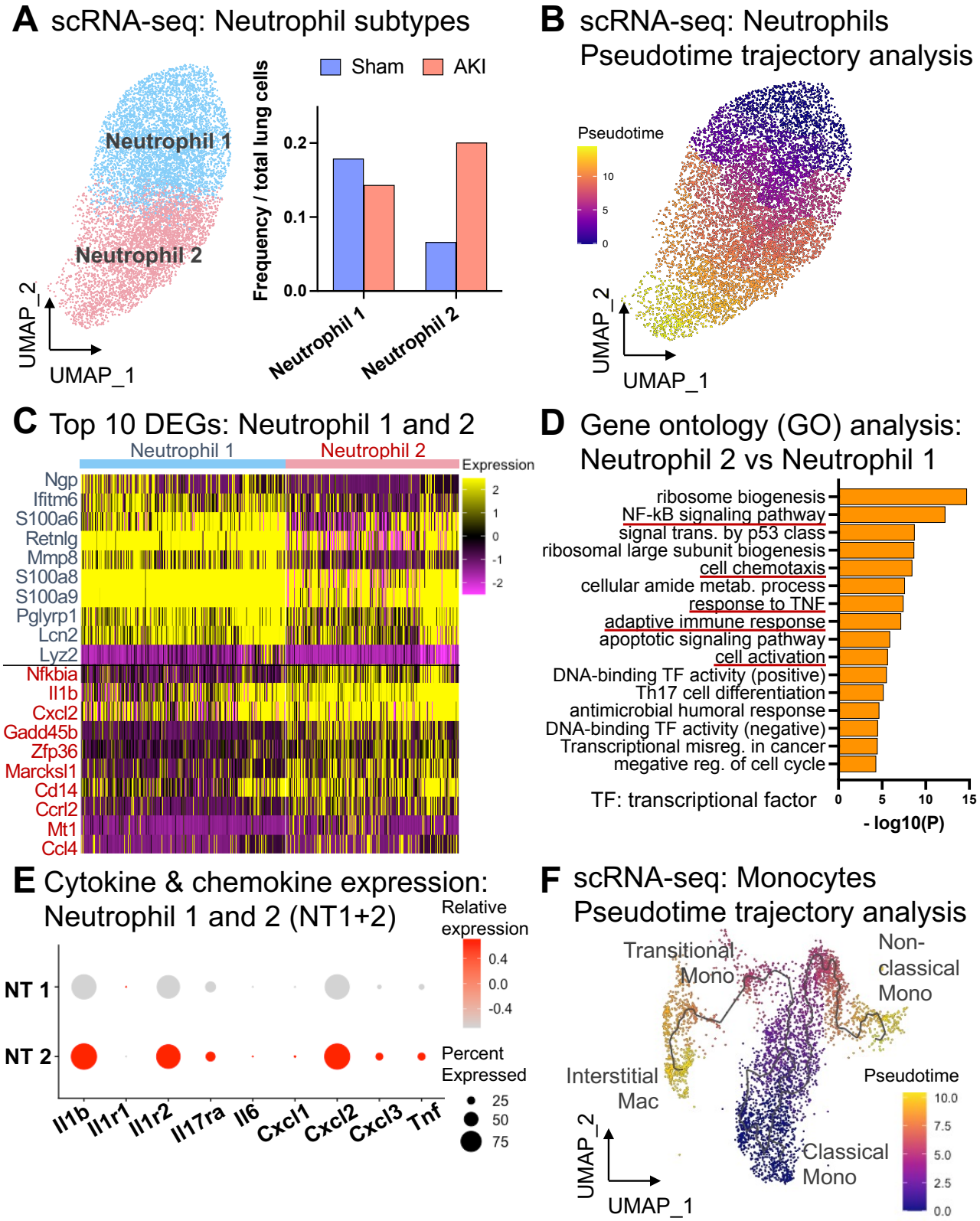

Fig.2. Sterile kidney tissue injury induces lung accumulation of activated neutrophils and monocyte-derived interstitial macrophages.
(A) UMAP representation of re-clustered lung neutrophil population only (3,807 sham and 5,770 AKI cells) yielded two distinct subtypes, neutrophil 1 and neutrophil 2. Quantification of the fraction of each neutrophil subtype sham vs AKI is shown in the graph. **(B)** Pseudotime trajectory analysis of neutrophils. **(C)** Top 10 differentially expressed genes (DEGs) neutrophil 1 vs. neutrophil 2. Ranking is created according to the relative fold change of gene expression. **(D)** Gene ontology (GO) analysis based on upregulated genes in neutrophil 2 over

neutrophil 1. GO terms associated with activation of neutrophils are underlined. **(E)** Expression levels of interleukins and chemokines across neutrophil subtypes 1 and 2. Dot size denotes percentage of cells expressing each gene and the color scale represents average gene expression levels. **(F)** Pseudotime trajectory analysis of monocytes, transitional monocytes, and interstitial macrophages in the lung.

Intravascular lung neutrophil accumulation and margination

During direct tissue injury neutrophils typically establish inflammation by extravasating from the circulation into the injured tissue (*20*, *21*), but whether this occurs in remote lung inflammation after sterile acute kidney tissue injury is unknown. Flow cytometry analysis of lung samples confirmed a significant increase in the total number of lung neutrophils after AKI, regardless of whether the lung samples were perfused with PBS or not at the time of sample preparation (**Figure 3A**). This suggested that neutrophils either extravasated into the lung interstitium or that they could not be flushed out due to strong vascular adhesion or vascular obstruction, such as by thrombus formation. To determine the localization of neutrophils, we carried out an *in vivo* neutrophil extravasation assay to distinguish between intravascular and extravasated neutrophils using two anti-Ly6G antibodies conjugated with different fluorochromes, as previously described (*22*). Firstly, an APC-labeled anti-Ly6G antibody was intravenously injected 10 minutes prior to sacrifice, and a second BV421-labeled anti-Ly6G antibody was added to lung single cell samples generated from the same animal after sacrifice. Only intravascular neutrophils would be double positive ($APC^+/BV421^+$), while extravasated neutrophils would be single positive ($BV421^+$), as they would only have been exposed to the second Ly6G antibody (**Figure 3B**). We used direct lung injury by intratracheal instillation of lipopolysaccharide (LPS) as a positive control for neutrophil extravasation. Following AKI, the total number of neutrophils in the lung significantly increased over sham levels and was comparable to the increase observed after direct lung injury with LPS. However, after AKI >99.5% of neutrophils remained marginated within the intravascular compartment in contrast to direct lung injury where over 80% of neutrophils were found extravasated (**Figure 3C,** quantification in **3D-3E**). Sterile kidney tissue injury-recruited lung neutrophils may therefore indeed impede blood flow in lung vessels.

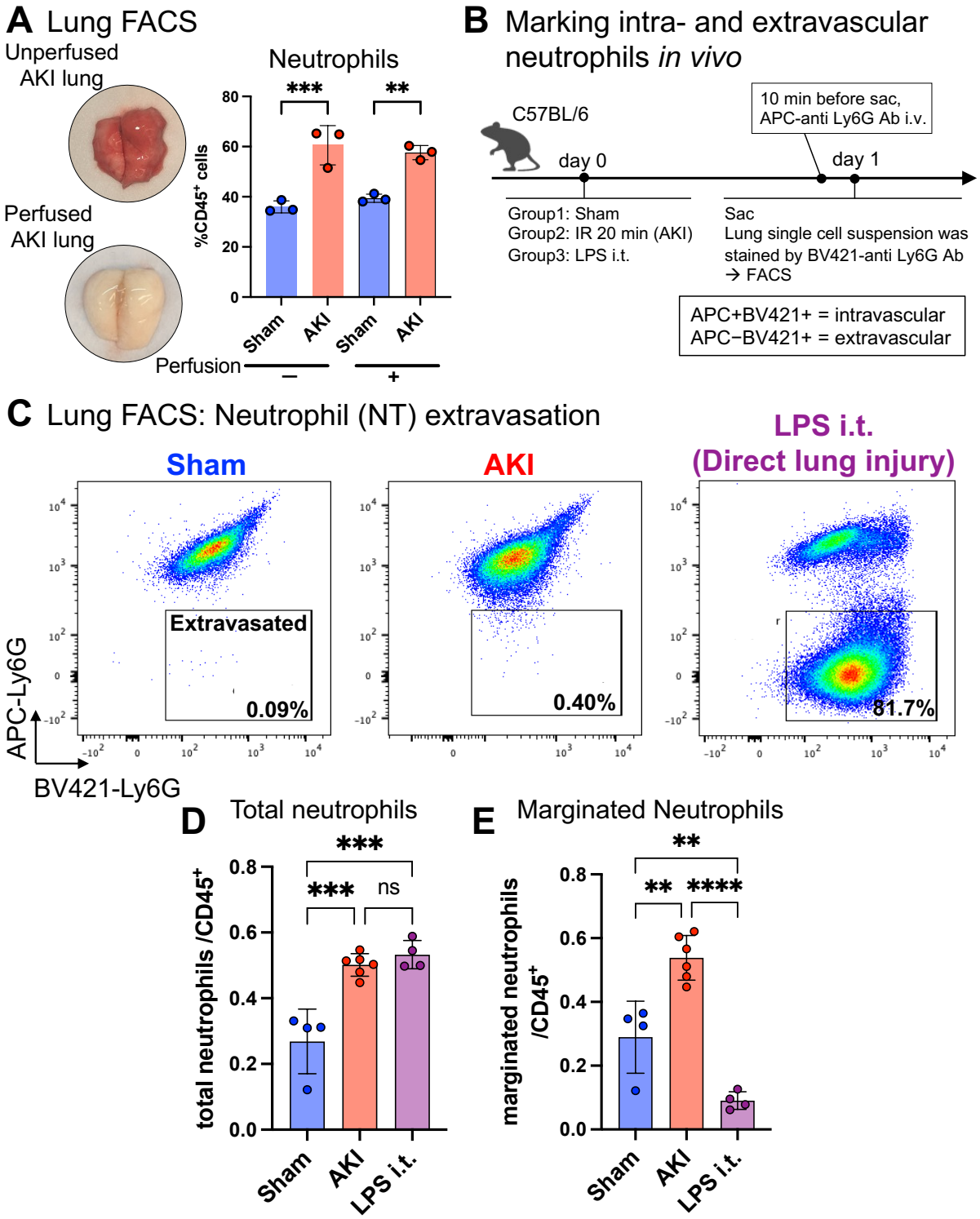

Fig.3. Intravascular lung neutrophil accumulation and margination.
(A) Representative image of mouse lung before and after perfusion with Phosphate-buffered saline (PBS). Total neutrophil count in sham vs AKI lung were quantified by flow cytometry (FACS) with or without prior lung perfusion. Neutrophils/CD45$^+$ cells: unperfused, 36.0% vs 60.5%; perfused, 39.4% vs 57.6%; in both sham vs AKI, $p < 0.01$. **(B)** Schematic of the *in vivo* neutrophil extravasation assay using two different anti-Ly6G antibodies coupled to different fluorescences (APC or BV421). **(C)** Identification of extravasated neutrophils by FACS. Ly6G fluorescence (APC over BV421) is analyzed in CD45$^+$, CD11b$^+$, Gr1^{high} cells in sham animals (left panel), AKI animals (middle panel), and animals subjected to direct lung injury by intratracheal (i.t.) lipopolysaccharide (LPS); single positive cells (BV421) are extravascular, double positive cells (APC/BV421) intravascular, **(D)** FACS quantification of total and **(E)** marginated (intravascular) lung neutrophils (both after

147 PBS perfusion). Data in (A, D, E) represent mean ± SD and n = 3 to 6 mice per group. ns: not significant. **P <
148 0.01, ***P < 0.001, ****P < 0.0001
149

150 **Intravascular lung capillary neutrophil train formation and thrombosis reduce lung**
151 **capillary perfusion**

152 To determine early events that establish remote lung inflammation after sterile kidney tissue
153 injury and its dynamics in real time, we investigated lung monocyte and neutrophil behavior in
154 the lung vasculature using intravital two-photon microscopy at two hours after injury as
155 compared to uninjured sham control. We used CCR2-GFP mice that allow *in vivo* tracking of
156 classical monocytes via GFP fluorescence (green). Neutrophils, blood flow and vessels were
157 visualized *in vivo* by i.v. injection of a fluorescence labeled anti-Ly6G antibody (red), of 1-
158 micron fluorescent microbeads (white), and of Qtracker655 (violet), respectively. Two hours
159 after sham operation few neutrophils, very few static microbeads, and few classical monocytes
160 were detected in the lung. Classical $CCR2^+$ monocytes were largely localized at a significant
161 distance from neutrophils (**Movie S1**). Two hours after AKI as compared to sham we found the
162 following: Lung neutrophils increased very significantly and swarmed lung capillary vessels
163 forming what could be described as "neutrophil trains", generally tightly associated with at least
164 one classical monocyte (see inset on right) (**Figure 4A** and **Movie S2**). Average distance
165 between classical monocytes and neutrophils was significantly reduced (**Figure 4B**),
166 intravascular neutrophil speed was significantly decreased (**Figure 4C**) and the presence of a
167 large number of intravascular immobile 1-micron beads suggested severely reduced blood flow
168 in the lung capillary microcirculation (**Figure 4D**). In some lung areas that contained extensive
169 neutrophil trains the vascular dye signal (Qtracker655, violet) was also visibly reduced or
170 showed discontinuity (**Figure 4A** see area in and around inset and **Movie S2**), also suggesting
171 reduced or disrupted capillary flow. Consistent with this, in AKI but not in sham lungs we
172 detected lung capillary micro-thrombosis by anti-platelet (CD41a) and anti-fibrinogen
173 immunofluorescence co-staining, covering about 6% of the lung area (**Figure 4E**). Taken
174 together, our findings thus indicate that neutrophil trains are blood flow impeding and that this
175 reduced blood flow is associated with thrombosis. Since ventilation is not impaired in remote
176 lung inflammation after AKI because alveolar exudates are largely missing (*10*, *11*, *14*), vessel
177 occlusion and reduced blood flow in perialveolar capillaries across larger areas of the lung, here
178 detected by intravital imaging in relatively superficial subpleural perialveolar capillaries, would
179 be expected to reduce blood oxygenation (ventilation-perfusion deficit). Such a ventilation-

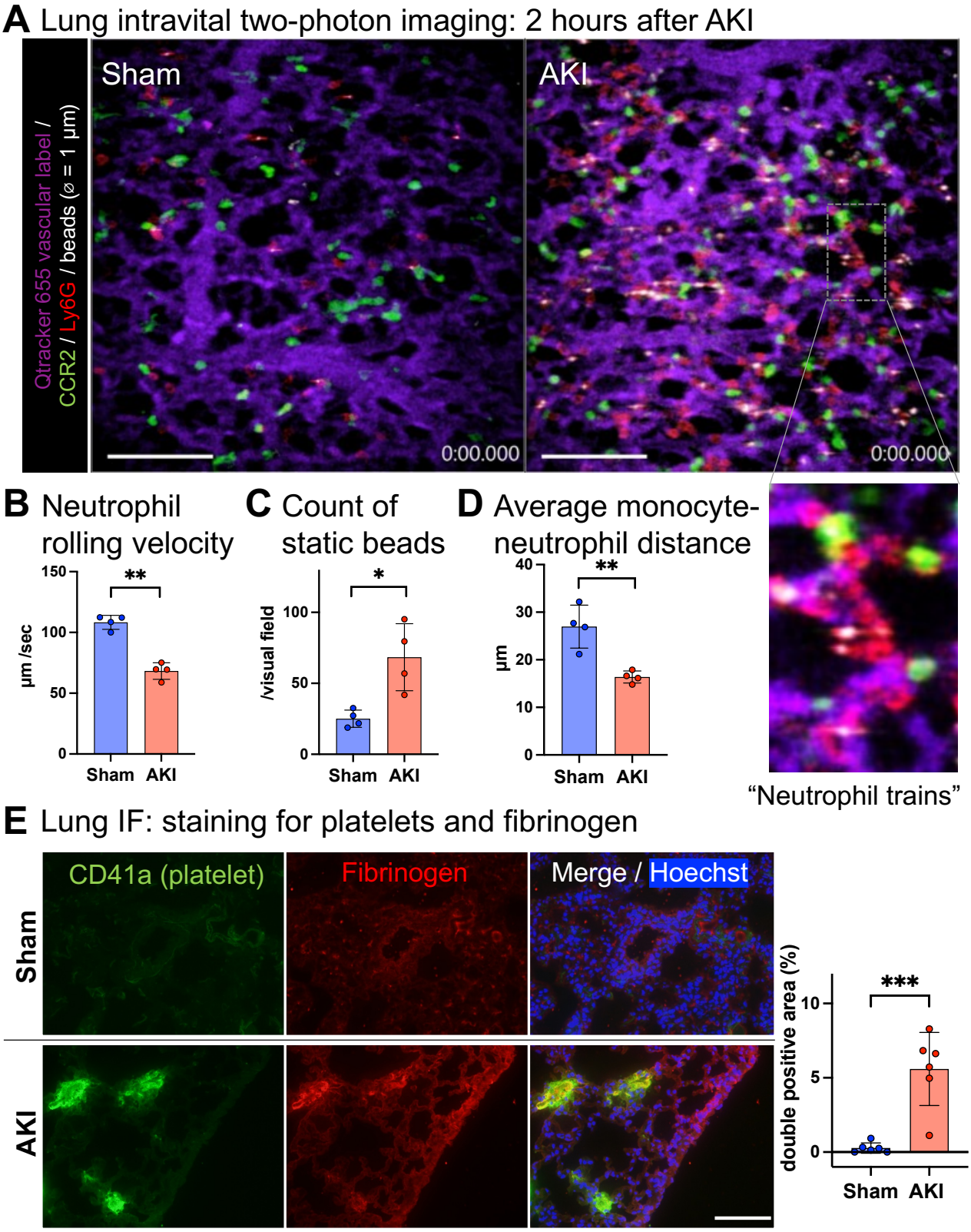

perfusion deficit would explain the hypoxemia we previously reported in these mice at 24 hours after AKI (*14*).

Fig.4. Intravascular lung capillary neutrophil train formation and thrombosis after AKI. **(A)** Intravital two-photon imaging of sham or AKI lungs 2 hours after AKI using CCR2-GFP mice and in vivo staining of neutrophils; $CCR2^+$ monocytes (green), $Ly6G^+$ neutrophils (red). Blood flow is assessed with 1-micron beads (white) and lung capillary microcirculation is labeled with intravenous injection of quantum dots (purple).

186 Magnified inset image shows a "neutrophil train" in a lung capillary, illustrating vessel occlusive accumulation of
187 neutrophil "train cars" attached to $CCR2^+$ monocyte "locomotives". Full videos are available in supplementary
188 materials. Scale bar = 100 µm. **(B-D)** Quantification of intravital imaging videos: speed of neutrophil rolling (B),
189 the number of static beads (C), and the averaged distance between $CCR2^+$ monocytes and neutrophils (D). **(E)**
190 Immunostaining for $CD41a^+$ lung platelets (green) and fibrinogen (red); graph shows quantification of double
191 positive area after sham or AKI. Hoechst 33342 dye (blue) was used to visualize nuclei. Scale bar = 100 µm. Data
192 in (B-E) represent mean ± SD and n = 4 to 6 mice per group. *P < 0.05, **P < 0.01, ***P < 0.001 compared to
193 sham.

194 **Rapid lung capillary neutrophil capture is enhanced by decreased neutrophil deformability**
195 **but does not depend on classical neutrophil-endothelial cell interactions**

196 Circulating neutrophils can be attracted to sites of inflammation based on identifiable sequential
197 interactions of different neutrophil cell surface ligands with endothelial cell surface receptors,
198 encompassing steps of neutrophil capture, rolling, crawling, arrest, and migration, prior to
199 potential extravasation (*23*). How neutrophils are recruited to the lung after remote sterile tissue
200 injury is however largely unknown. Based on our observations of neutrophil crawling/arrest in
201 intravital imaging, we tested blockade of key neutrophil-endothelial cell interactions that mediate
202 neutrophil crawling/arrest and migration. The integrins LFA-1 (CD11a/CD18) and Mac-1
203 (CD11b/CD18) play overlapping roles in neutrophil arrest and migration (*23*, *24*). Their
204 endothelial receptor ICAM-1 is upregulated in lung endothelium on Day 1 after AKI, in
205 particular in venous endothelial cells (**Figure 5A**), where transmigration of neutrophils would
206 predominantly occur (*23*). However, blockade of CD18 (**Figure 5B**) or of LFA-1 (**Figure S1**)
207 did not reduce early neutrophil recruitment into the lung at two hours after AKI. We thus
208 hypothesized that due to its very rapid onset (<1 hour) (*14*) neutrophil recruitment to the lung
209 after sterile kidney tissue injury may not depend on a specific capture signal that emanates from
210 the lung. This hypothesis was further guided by the knowledge that the lung capillary diameter is
211 on average 7.5 microns in diameter (*24*, *25*), significantly smaller than neutrophils and
212 monocytes, which have an average size of 9-15 microns in diameter (*24*). Thus, neutrophils have
213 to be deformable to pass the lung vasculature. Primed/activated neutrophils are known to be less
214 deformable (*26*) due to changes in their cellular shape induced by cytoskeletal rearrangement
215 with the hallmark formation of polymerized F-actin bands in sub-cell membrane regions (*27*).
216 We therefore examined cell shape and presence of F-actin bands in neutrophils after sterile
217 kidney tissue injury as compared to sham. Lung images obtained by electron microscopy (EM)
218 confirmed the intravascular neutrophil accumulation phenotype seen with intravital imaging.
219 Cell shape was determined by measuring and comparing the ratio of longest short to longest long

220 neutrophil axis. At Day 1, we detected mostly empty vessel lumen (arrows) and few neutrophils
221 (full arrowhead) in sham lungs, and most neutrophils had a deformable elongated cellular shape
222 with smooth cellular surface and no obvious interaction with endothelium (**Figure 5C**, upper
223 images and graph). Mice with acute kidney tissue injury showed an increased number of
224 neutrophils within the vasculature (full arrowheads) that exhibited a less/non-deformable
225 rounded shape showed significant interactions with the endothelium (**Figure 5C**, lower images
226 and graph). These visible interactions correspond to tethers/slings of adhesive neutrophils that
227 interact with the endothelial wall (*28*), suggesting they were crawling or arrested on
228 endothelium, and confirming our findings in intravital imaging (Figure 4). As seen in intravital
229 imaging, monocytes (open arrowhead) were detected tightly associated with "neutrophil train"
230 cars (closed arrowheads) in EM (**Figure 5C** left lower image). Disruption of alveolar epithelium
231 or signs of endothelial apoptosis/necroptosis of cells was not evident in our analysis. Next we
232 visualized F-actin polymerization and peripheralization using phalloidin staining in circulating
233 neutrophils isolated from sham or AKI mice, using FACS analysis and IF staining. Flow
234 cytometry detected significantly increased F-actin fluorescence in neutrophils 4 hours after AKI
235 compared to sham (**Figure 5D**). By IF staining 20% of circulating neutrophils isolated from
236 sham animals showed sub-cell membrane F-actin bands, whereas in AKI animals sub-cell
237 membrane F-actin bands were detected in 30% of neutrophils at 2 hours, and 40-50% at 4 hours
238 (**Figure 5E)** and on Day 1 after AKI (**Figure S2**); these numbers are very likely an
239 underestimate since many non-deformable neutrophils would be trapped in the lung and not
240 freely circulating. The massive rapid recruitment of neutrophils to the lung after sterile kidney
241 tissue injury is thus strongly enhanced by neutrophil priming/activation by kidney injury-
242 released circulating factors that induce decreased deformability, and rapid capture of neutrophils
243 in lung capillary vessels.

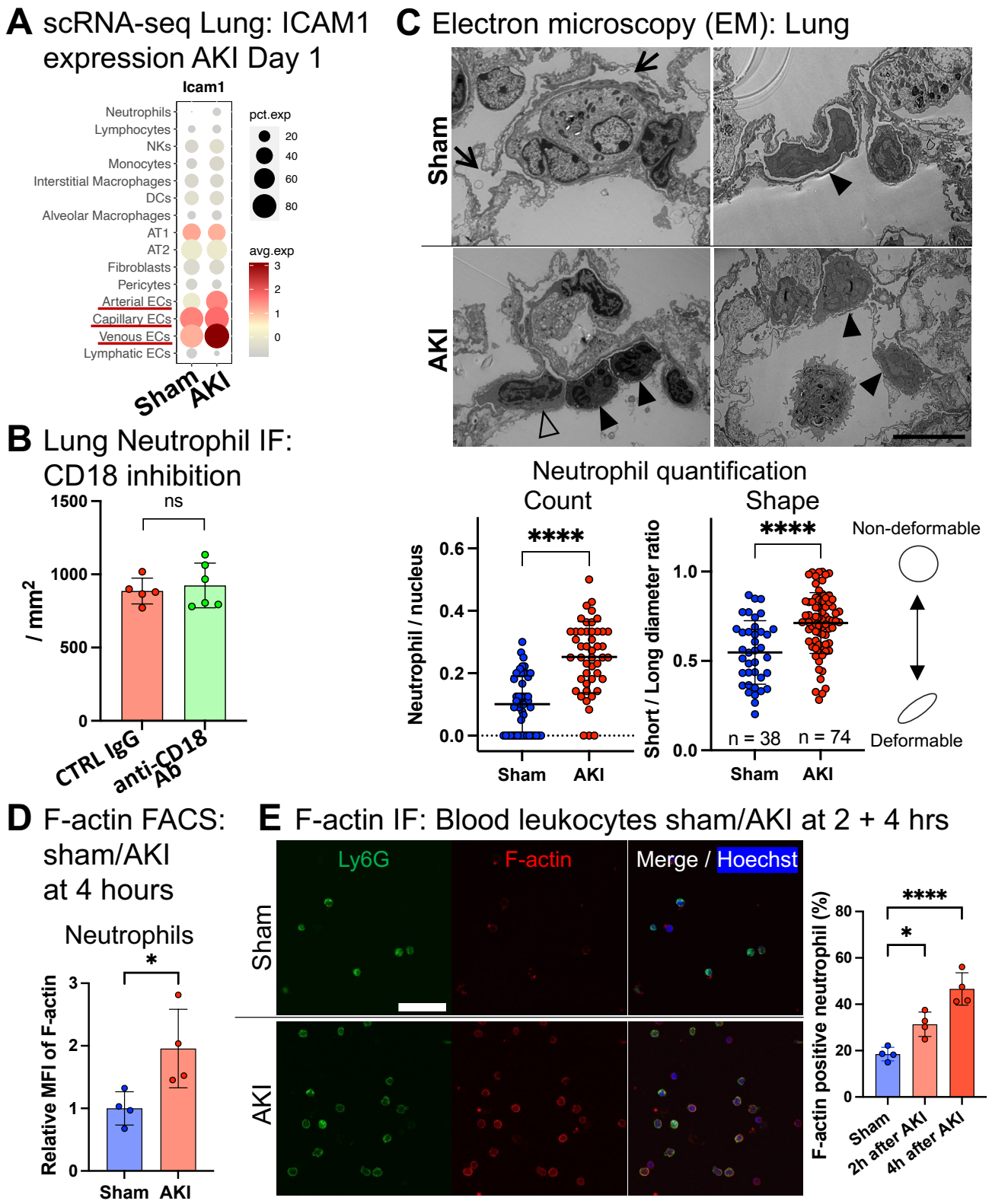

Fig.5. Rapid lung capillary neutrophil capture is enhanced by decreased neutrophil deformability but does not depend on classical neutrophil-endothelial cell interactions.
(A) Single-cell RNA seq analysis (see also Figure 1): Expression of adhesion molecule, ICAM1, in lung cell types after sham or AKI. The dot size denotes percentage of cells expressing each gene, and the color scale represents average gene expression levels. **(B)** anti-CD18 antibody blockade vs IgG control in C57/BL6 mice: Quantification of lung neutrophils by Ly6G immunofluorescence staining after AKI. **(C)** Representative images of sham vs AKI lung obtained by electron microscopy (EM) with quantification (graphs). Arrows indicate empty vessel lumen,

while full arrowheads point out deformable neutrophils in sham or non-deformable neutrophils in AKI lung; in the AKI lung an open arrowhead is pointing out a monocyte "locomotive" leading non-deformable neutrophil train cars. Right lower image shows crawling or arrested neutrophils (closed arrowheads). EM images were obtained from 3 mice/group for sham and AKI. Scale bar = 10 µm. Left graph: neutrophil count is presented as number of neutrophils per total nuclei in each image. Right graph: the ratio of short over long diameter in each neutrophil is shown as an indicator of its morphology. Short/long ratio closer to 1.0 means a more rounded non-deformable shape. **(D)** Quantification of F-actin in circulating neutrophils by flowcytometry. Using fluorescently-labeled phalloidin, geometric mean fluorescence intensity (MFI) is analyzed and compared between sham vs AKI. **(E)** F-actin staining of leukocytes isolated from circulating blood 2 and 4 hours after sham or AKI. Scale bar = 40 µm. Percentage of F-actin polymerized $Ly6G^+$ cells (neutrophils) are quantified in graph. n = 4-6 mice/group. Data represent mean ± SD. ns: not significant, *P < 0.05, ****P < 0.0001

$CCR2^+$ classical monocytes and CXCL2 drive lung capillary neutrophil swarming

We next aimed to elucidate how captured neutrophils are retained in the lung to form neutrophil trains. Since classical monocytes were the other significant immune cell population that increased after sterile kidney tissue injury (**Figure 1D**) and they appeared to interact with neutrophils based on intravital imaging and EM in lung capillaries, we examined their role in establishing lung capillary neutrophil trains. First, we selectively depleted $CCR2^+$ classical monocytes by administration of anti-CCR2 antibody (*29*) (**Figure 6A**). This antibody does not deplete circulating neutrophils (*30*). Anti-CCR2 antibody pre-treatment depleted classical monocytes ($CD11b^+$, $Ly6G^-$, $CCR2^+$, $Ly6C^+$) but not non-classical monocytes ($CD11b^+$, $Ly6G^-$, $Ly6C^-$) (**Figure 6B**), and no difference in kidney injury between anti-CCR2 or control-antibody treated animals (serum blood urea nitrogen (BUN)) was observed (**Figure 6C**). However, depletion of classical monocytes almost completely blocked lung neutrophil and interstitial macrophage accumulation after AKI (**Figure 6D**). These results identify classical $CCR2^+$ monocytes as key upstream players in lung neutrophil accumulation after AKI and as the source of lung interstitial macrophages. In contrast, genetic deficiency of non-classical monocytes in NR4A1 knock-out mice (*31*) (**Figure 6E**) did not prevent lung neutrophil or interstitial macrophage accumulation (**Figure 6F**). We next attempted to infer the involved classical monocyte-derived neutrophil chemoattractant signals by analyzing lung cell-cell communication using lung scRNA-seq data (see Figure 1) analysis with CellChat, a software platform that predicts intercellular communication networks based on expression data of known ligand-receptor pairs. The total number of inferred signaling interactions in the lung vascular niche between neutrophils, monocytes, transitional monocytes and their interstitial macrophage progeny, and endothelial cells modestly increased after AKI (~5%) (**Figure 6G**). Cell-cell communication analysis comparing sham control with AKI predicted a strong relevance of classical monocyte to neutrophil signaling via the neutrophil chemoattractant CXCL2 acting on

287 CXCR2 receptor expressed in neutrophils after sterile kidney tissue injury (**Figure 6H**). Injection
288 of CXCL2 neutralizing antibody in AKI animals as compared to IgG control significantly
289 suppressed neutrophil accumulation and neutrophil train formation in the lung (**Figure 6I**).
290 Taken together, these findings suggest that $CCR2^{+}$ classical monocyte-derived CXCL2 signaling
291 is critical for lung capillary neutrophil train formation after sterile kidney tissue injury. A
292 summary of our findings is shown in **Figure 7**.

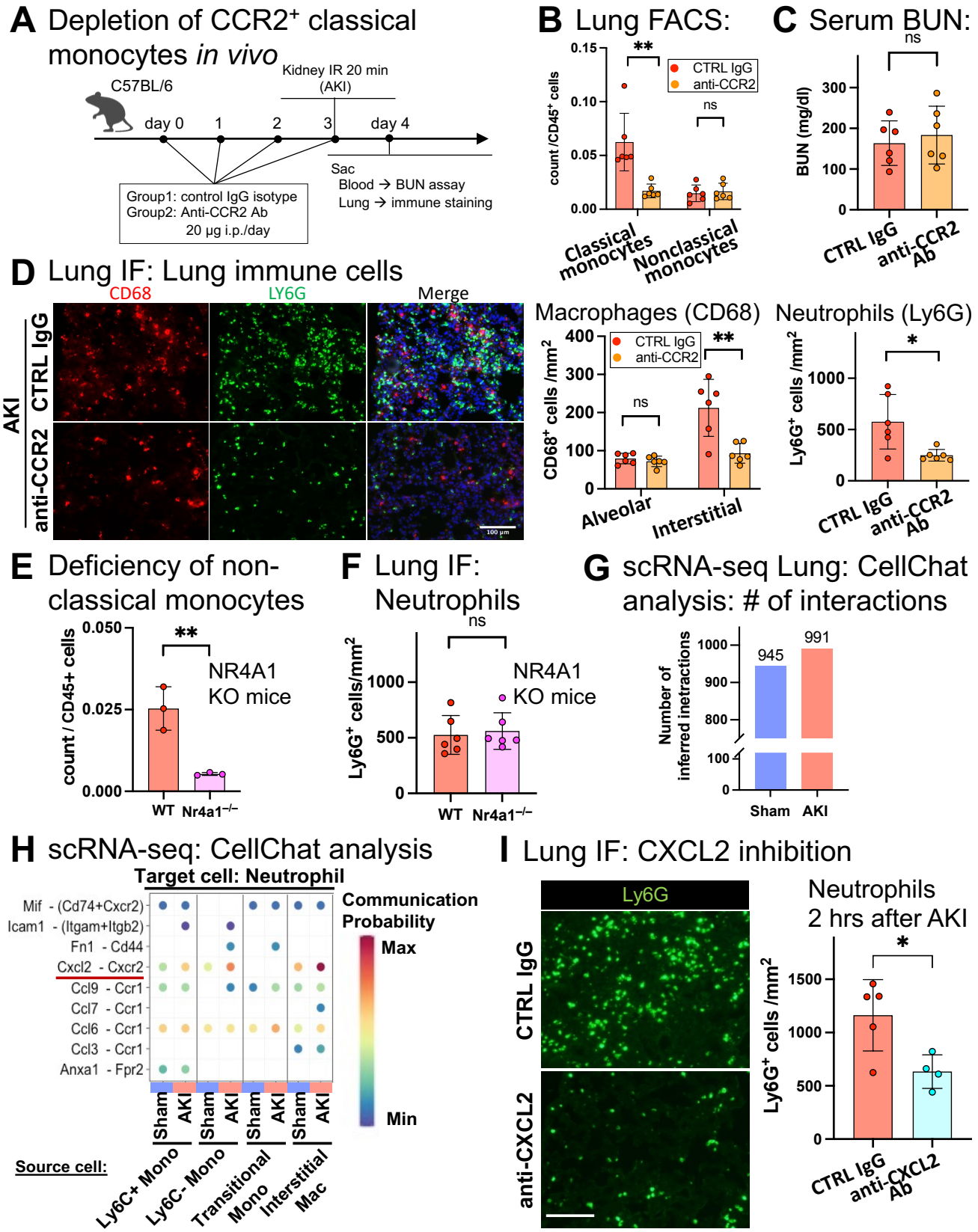

Fig.6. CCR2+ classical monocytes and CXCL2 drive lung capillary neutrophil swarming. **(A)** Schematic of classical monocyte depletion using anti-CCR2 antibody in vivo. **(B)** Lung monocytes after pretreatment with anti-CCR2 antibody or control IgG. **(C)** Serum blood urea nitrogen (BUN): Kidney injury level on day 1 after AKI. **(D)** Lung immunofluorescence staining after AKI in control vs anti-CCR2 antibody-treated animals: alveolar and interstitial macrophages (CD68+, red) and neutrophils (Ly6G+, green). Hoechst 33342 dye

(blue) was used to visualize nuclei. Scale bar = 100 µm. **(E)** Quantification of Ly6C^{-} non-classical monocytes in wildtype vs NR4A1 knockout animals. **(F)** Quantification of lung neutrophils after AKI measured by immunofluorescence staining. **(G)** Total number of cell-cell communication inferred by CellChat based on scRNA-seq analysis sham vs AKI (also see Figure 1). **(H)** Cell-cell communications from monocytes or macrophages to neutrophils were predicted at single ligand-receptor resolution (unbiased); the neutrophil chemoattractant CXCL2 in monocytes/macrophages and its receptor CXCR2 in neutrophils were predicted as significantly increased in sham vs AKI and are underlined. **(I)** Lung immunofluorescence staining for Ly6G^{+} neutrophils (green) in wildtype C57/BL6 mice injected with anti-CXCL2 antibody or control antibody and subjected to AKI. Scale bar = 100 µm. Data represent mean ± SD and n = 3 to 6 mice per group. ns: not significant, *P < 0.05, **P < 0.01

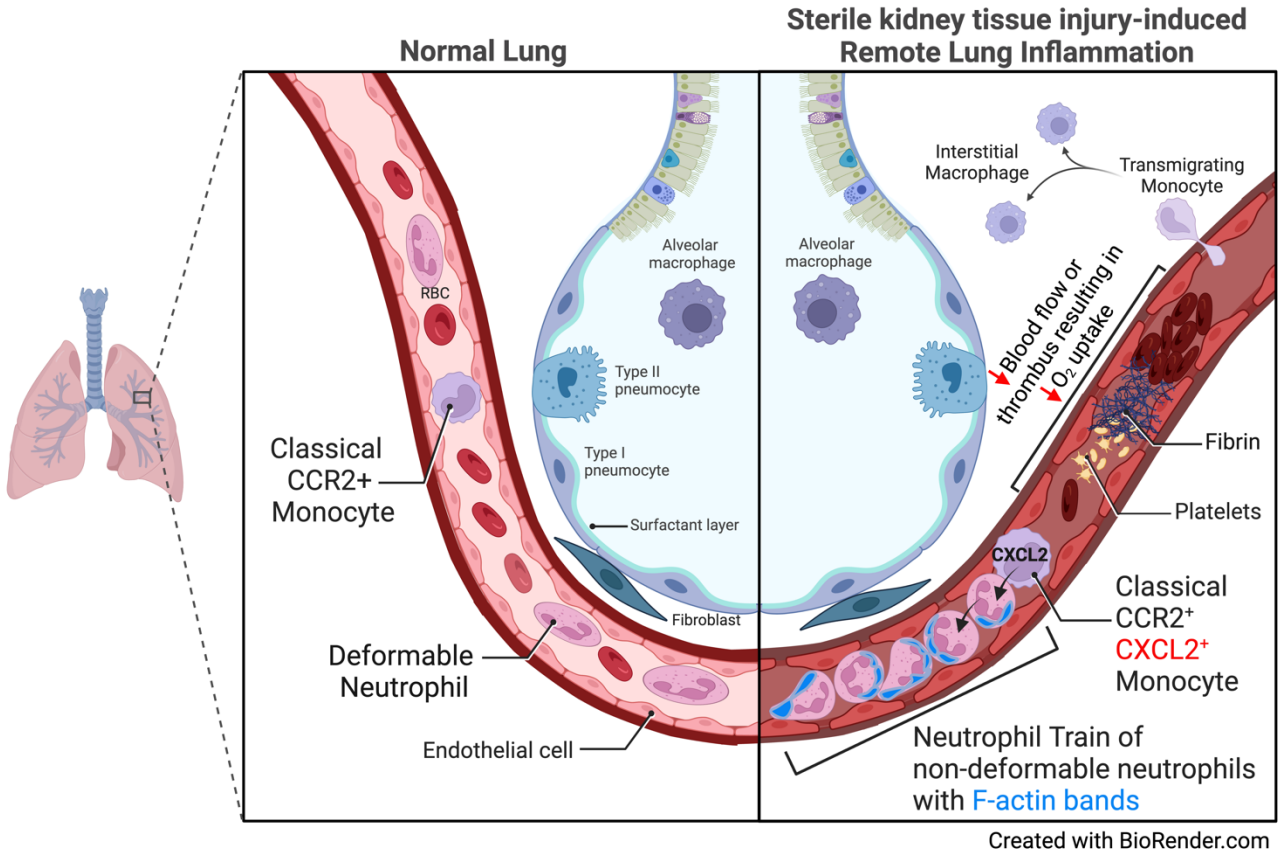

Fig.7. Summary

Sterile kidney tissue injury induces rapid intravascular "neutrophil train" formation in lung alveolar capillaries, a novel form of neutrophil swarming. Rapid swarming is enhanced by decreased deformability secondary to F-actin polymerization (submembrane F-actin bands) in circulating neutrophils that impedes their lung capillary passage. CCR2^{+} classical lung monocytes are required for neutrophil train formation and release CXCL2 to attract neutrophils into neutrophil trains. Neutrophil train formation reduces alveolar capillary blood and is associated with thrombosis (thrombi contain both platelets and fibrin). This capillary perfusion deficits leads to reduced oxygenation despite proper alveolar function and ventilation, unlike in infectious inflammatory lung diseases, such as bacterial pneumonia.

317 **Discussion**

318 Our work reveals that sterile tissue injury induces a novel form of intravascular neutrophil
319 swarming, lung capillary "neutrophil trains", that severely impeded lung capillary blood flow
320 and led to associated microcirculatory thrombosis.

321 The normal lung circulation contains marginated intravascular neutrophils representing
322 up to 30% of the total circulating neutrophil pool and also classical and non-classical monocytes,
323 together forming an immune niche poised to rapidly respond to various immune challenges, in
324 particular the invasion of pathogens (*32*). 100% of right cardiac output passes through the lung,
325 such that during dissemination of infection via the bloodstream pathogens have to pass through
326 the lung. Like sepsis, sterile acute kidney tissue injury induces a systemic inflammatory response
327 syndrome (SIRS) involving many the same circulating pro-inflammatory mediators, and also
328 increases in circulating neutrophils and monocytes (*10*). Pathogens in the bloodstream induce the
329 formation of sizable lung intravascular neutrophil swarms in larger caliber lung vessels that
330 facilitate pathogen capture and clearance and serve as an important evolutionarily conserved
331 defense mechanism against sepsis (*33*). We show that lung neutrophil trains induced by sterile
332 tissue injury differ in that their primary location is in alveolar capillaries in which blood flow is
333 required for oxygen exchange. We thus speculate that lung capillary intravascular neutrophil
334 train formation and slowed lung capillary blood flow after sterile tissue injury may serve to
335 sequester activated immune cells and circulating cytokines in the lung, protecting the organism
336 from their overt systemic action, but at the expense of causing blood oxygenation deficits that
337 can cause or enhance hypoxemia. Extensive sepsis-induced neutrophil swarming can indeed
338 negatively impact oxygenation (*34*). Widespread medium to large vessel arterial and venous
339 thrombosis containing neutrophil macroaggregates has been described after gut ischemia in mice,
340 and also in patients with severe acute respiratory distress syndrome (ARDS) (*16*).

341 While neutrophil accumulation in the lung after sterile acute kidney tissue injury in mice
342 has been described previously (reviewed in (*10*)), their rapid capture in the lung due to tissue
343 injury-induced decreased deformability and the formation of intravascular lung capillary
344 "neutrophil trains" was unknown prior to our studies. Changes in neutrophil deformability (*35*)
345 and lung retention lasting >40min has been observed in humans following the injection of *ex*
346 *vivo* primed neutrophils (*36*), and changes in flow and adhesive properties ("stiffening") of
347 circulating immune cells have also been shown in humans with trauma (*37*), acute respiratory
348 distress syndrome (ARDS) (*38*), cardiac tissue injury (*39*), or sepsis (*40*, *41*). We showed that the

349 known canonical steps of neutrophil recruitment that mediate neutrophil crawling/arrest and
350 involve defined neutrophil/endothelial interactions, such as LFA-1/ICAM1 or Mac-1/ICAM1
351 interactions, are not involved in lung neutrophil recruitment after acute sterile kidney tissue
352 injury. This is not unprecedented as neutrophil recruitment is strongly context dependent (*33*)
353 and non-canonical pathways involved in neutrophil recruitment have been described in different
354 tissues (*42*). As example, lung neutrophil recruitment in streptococcal pneumonia (direct lung
355 injury) is unaffected by deficiency of E- or P-Selectin (*43*), endothelial proteins that mediate
356 neutrophil capture/rolling in the canonical pathway but is dependent on Mac-1 (CD11b/CD18)
357 (*32*).

358 The observed differences of neutrophil swarms after sepsis as compared to sterile tissue
359 injury suggest different mechanisms are involved in their formation. In several contexts,
360 leukotriene-B-4 (LTB-4) is required for the initiation of intravascular neutrophil swarming and
361 clustering behavior (reviewed in (*33*)), in particular in fungal sepsis (*34*). However, we did not
362 find any significant expression of LTB-4 in lung cells after sterile kidney tissue injury. Instead,
363 our model supports the involvement of the neutrophil chemoattractant CXCL2 as the signal that
364 retains captured neutrophils in the lung. CXCL2 has not been directly linked to lung neutrophil
365 recruitment after acute kidney tissue injury, but mice deficient in the CXCL1/2 receptor CXCR2
366 or mice treated with anti-CXCL1 antibody show reduced remote lung neutrophil recruitment (*44*)
367 after sterile kidney tissue injury, supporting our data. As demonstrated by intravital imaging 2
368 hours after sterile kidney tissue injury, monocyte released CXCL2 is important in the formation
369 of neutrophil trains very early after AKI. At late time points after, as our cell-cell communication
370 analysis on Day 1 after injury suggests, neutrophils produce CXCL2 themselves, likely
371 contributing to increased "neutrophil train" length and lung neutrophil retention.

372 A role of monocytes in lung neutrophil recruitment and extravasation different from
373 sterile tissue injury has been demonstrated in direct lung injury with bacterial challenge and in
374 lung ischemia reperfusion injury(*45*); the latter naturally occurs during lung transplantation.
375 Here, IL1b released by intravascular non-classical monocytes acts on alveolar macrophages to
376 release CCL2, which in turn attracts $CCR2^+$ classical monocytes that drive IL1b-dependent
377 neutrophil extravasation (*46*) (reviewed in (*47*)). In a separate role, $CCR2^+$ monocytes in our
378 model also extravasate into lung tissue and develop into lung interstitial macrophages. The
379 mechanistic role of these interstitial macrophages remains to be determined, but we speculate
380 that they have a protective repair function.

381 Sterile tissue injury-induced lung neutrophil trains and capillary flow obstruction could
382 explain the profound hypoxia we previously observed in our sterile kidney tissue injury model
383 despite the surprising absence of alveolar exudates and intact alveolar epithelium(*14*). Our
384 findings provide an alternate explanation for respiratory failure in the context of acute kidney
385 injury (AKI) in patients, whether it occurs isolated or as part of existing respiratory failure from
386 primary or secondary causes (such as COVID-19, bacterial pneumonia, sepsis or trauma). In AKI
387 patients, respiratory failure is often attributed to volume overload with left ventricular failure and
388 lung interstitial edema, despite the fact that these patients frequently exhibit normal wedge
389 pressure on cardiac catheterization (*48*, *49*) and do not significantly improve with dialysis and
390 volume removal (*12*). Increased wedge pressure signals reduced left ventricular function and
391 "blood backup" into the lung, causing reduced lung capillary flow and oxygenation. That AKI
392 causes a similar capillary flow and oxygenation problem is the novelty of our findings. Strategies
393 to detect and prevent remote lung inflammation and lung capillary neutrophil train formation
394 may represent novel therapeutic avenues to diminish or prevent AKI-induced respiratory
395 complications in the clinic.

396 **Materials and Methods**

397 **Animal experiments**

398 8–12-week-old male mice were used for all experiments in accordance with the animal care and
399 use protocol approved by the Institutional Animal Care and Use Committee of Washington
400 University School of Medicine (protocol #19-0044 and #22-0105). C57BL/6J (strain #000664)
401 and NR4A1-KO (#006187) mice were purchased from The Jackson Laboratory (Bar Harbor,
402 ME) and kept in 12 hours-light/dark cycle with liberal water and standard chow diet. In our AKI
403 model 20-minutes of bilateral ischemia/reperfusion (IR) injury was introduced at 37°C using the
404 flank approached as previously described (*14*). Sham operation was performed using the same
405 surgical procedure without clamping the renal hilum with surgical clips. In select experiments,
406 following intubation with a 20G catheter, 0.1 μg/g of lipopolysaccharide (LPS) derived from
407 *Pseudomonas aeruginosa* (Sigma-Aldrich #L8643) was instilled intratracheally to induce direct
408 lung injury. For $CCR2^+$ monocyte depletion, C57BL/6J mice were injected with anti-CCR2
409 antibody (MS-21) 20 μg per day for four consecutive days (*29*, *50*) prior to IR injury. For
410 CXCL2 inhibition, a total of 100 μg of anti-CXCL2 monoclonal antibody (Invitrogen MA5-
411 23737) was injected (50 μg i.p. 1 hour prior to ischemia and another 50 μg i.v. at reperfusion).
412 Control animals were treated with the same dosage of rat IgG isotype (Invitrogen #10700). The
413 organs were harvested 2 or 24 hours after IR injury, as specified in each experiment.

414 **Single-cell preparation from mouse lung and kidney**

415 Twenty-four hours after sham or AKI surgery, mice were euthanized and perfused with 20 ml of
416 ice-cold PBS from the left and right ventricles to remove remaining blood in the lung
417 vasculatures. Perfused lung was immediately dissected and chopped into <1mm^3 dices by
418 scalpels and razors. For single cell preparation samples were incubated for 60-min at 37°C with
419 gentle shaking in RPMI media supplemented with 50 mg/ml of Liberase TL (Roche
420 #5401020001), 40 U/ml of DNAse I (Sigma-Aldrich #D4527), and 0.75 mg/ml of hyaluronidase
421 (Sigma-Aldrich #H3506). At the end of incubation each sample was filtered twice, once through
422 a 70 mm and once through a 40 mm strainer. Red blood cells in the samples were removed by
423 ACK lysing buffer (Quality Biological #118156101). Single-cell suspensions were then washed
424 and resuspended in FACS buffer (PBS, 0.5% BSA, 2mM EDTA, 0.01% NaN_3), and used for
425 single-cell RNA sequencing (scRNA-seq) and/or flow cytometry analysis.

426 **Single-cell RNA sequencing (scRNA-seq) and data analysis**

427 scRNA-seq analysis was conducted on lung and kidney samples from sham and AKI as
428 previously described (*14*). Briefly, a total of four samples were pooled for each group and live
429 cells were sorted using propidium iodide staining using a FACSAria III (BD Biosciences) flow
430 cytometer. cDNA libraries were prepared using the Chromium Single Cell 5' Library Kit v2 (10x
431 Genomics, Pleasanton, CA) following manufacturer's instructions. The amplified full-length
432 cDNA libraries were then submitted to the Genome Technology Access Center of Washington
433 University for sequencing, with a sequencing depth of 50,000 reads. All subsequent data
434 processing steps were performed using R software (v4.1.0) with Seurat v4 (*17*). Expression
435 matrices for each sample were imported into R as Seurat objects. Quality control was initially
436 performed by retaining cells with gene expression counts ranging from 200 to 3200. Cells with
437 more than 10% mitochondrial genes and genes not expressed in at least three cells were
438 excluded. After these quality control steps, the SCTransform and Harmony functions were
439 employed for normalization, scaling, variance stabilization, and integration of the datasets (*51*,
440 *52*). After quality control and integration, we performed clustering by applying a K-nearest
441 neighbor graph with a resolution of 0.2 on the result of principal component analysis (PCA). We
442 visualized the clustering using uniform manifold approximation and projection (UMAP). To
443 assign cluster identities, we first compiled a list of lung and kidney cell types and their currently
444 established markers (*18*, *53*) and performed manual annotation using those markers and
445 additional differentially expressed genes (DEGs) between clusters identified by the
446 FindAllMarkers() function of Seurat. Functional properties of DEGs were then investigated by
447 GO term analysis using Metascape (*54*). The expression levels of genes of interest in each cluster
448 were visualized using 'plot1cell' package (*55*). For trajectory analysis to assume pseudotime
449 between different subtypes in UMAP we used the Monocle 3 program (*56*). Cell-cell
450 communication analysis within the scRNA-seq datasets was performed using CellChat (*57*). The
451 mouse scRNA-seq datasets used in this paper have been uploaded and are available under the
452 GEO accession number GSE249928.

453 **Flowcytometry analysis**

454 Single-cell suspensions were stained with LIVE/DEAD Aqua cell dye (Invitrogen #L34965,
455 dilution 1:200) for 30 minutes. After washing with PBS, FcR blocking with anti-mouse-CD16/32
456 antibody (BioLegend #101302, dilution 1:100) was performed for 15 minutes in FACS buffer,
457 followed by 30-min incubation with the following diluted antibodies: BV605-anti-mouse CD45
458 (BioLegend #103139, 1:200), BV421-anti-mouse Ly6G (BioLegend #127627, 1:200), BUV395-
459 anti-mouse CD11b (BD Biosciences #563553, 1:200), BV786-anti-mouse SiglecF (BD

460 Biosciences #740956, 1:200), FITC-anti-mouse F4/80 (Invitrogen #11480181, 1:100), PE-anti-
461 mouse MERTK (BioLegend #151506, 1:100), APC-anti-mouse Ly6C (BioLegend #128016,
462 1:400). Unstained and single stained compensation samples were prepared from live lung or
463 spleen cells for each FACS run. For quantification of F-actin in neutrophils, blood leukocytes
464 were incubated with rhodamine-conjugated phalloidin (Invitrogen #R415, 1:200) for 30 minutes
465 at room temperature after permeabilization by 0.2% Tween-20. FACS analysis was performed on
466 BD Fortessa X20 with five lasers and data was analyzed with FlowJo software (BD, NJ).

467 **In vivo neutrophil extravasation assay**

468 In order to distinguish intravascular from extravasated neutrophils, 10 ml APC-anti-mouse-Ly6G
469 antibody (BioLegend, #127614) was intravenously injected 10 minutes before sacrifice as
470 previously reported (*22*). After dissociation of lungs into single cell suspensions, each sample
471 was stained by another anti mouse Ly6G antibody (BioLegend, #127627) carrying a different
472 fluorescence (BV421). During FACS analysis, intravascular neutrophils were identified as
473 double positive (APC^+, $BV421^+$), whereas extravasated neutrophils were single positive (APC^+,
474 $BV421^-$) since they were not reached by the intravenously applied first antibody.

475 **Intravital imaging of the lung**

476 Intravital lung imaging in CCR2-GFP mice was performed using two-photon microscopy as
477 previously described (*45*). Briefly, 1.5 hours after IR or sham surgery, mice were orotracheally
478 intubated with a 20 G catheter and ventilated with 1.5% isoflurane in air supplemented with
479 2L/min of oxygen (tidal volume: 220-250 µl, respiratory rate 250/min). To visualize neutrophils
480 after AKI or sham, blood vessels, and blood flow, 8 µL of PE-anti-mouse-Ly6G antibody
481 (BioLegend, #127608), 10 µL of 655-nm Q-dots (Invitrogen, #Q21021MP), and 5 µL of 1-µm
482 fluorescent beads (Invitrogen, #F13080) were intravenously injected prior to imaging. A
483 thoracotomy with partial removal of 4-5 left lower ribs exposed enough lung tissue for two-
484 photon microscope imaging. Our strategy allowed intravital lung imaging at about 2 hours after
485 sham or AKI. The video rate was set to 300 msec and six random areas of the lung were recorded
486 for at least 25 seconds per animal. The entire surgical and acquisition process was conducted on
487 a heated pad to maintain the body temperature of mice at 37°C. The acquired videos were
488 analyzed using the Imaris software version 9.8.2 (Oxford Instruments, Abingdon, UK).

489 **Immunofluorescence staining**

490 Lung histology was examined in fresh-frozen sections embedded into OCT compound (Fisher
491 #4585). 10 images/lung were collected for blinded quantification by experienced lab members.

492 OCT tissue cryo-sections were washed with PBST (0.05% Tween-20 in PBS) for 5 minutes at
493 room temperature and permeabilized with 0.1% Triton-X in PBS for 5 minutes, followed by
494 PBST washes (3 x 5 min). After 30 min incubation in blocking buffer (1% BSA and 10% normal
495 goat serum in PBS), sections were incubated with primary antibodies overnight at 4ºC, followed
496 by PBST washes (3 x 5 min), 1 h incubation at room temperature with secondary antibodies
497 (where appropriate), 5 min with Hoechst dye (Thermo #62249), followed by PBST washes (3 x
498 5 min) and mounting solution (2 mg/mL para-phenylenediamine) was applied. Primary Abs:
499 anti-mouse-Gr-1 (FITC-conjugated, eBioscience, , #14-5931), rabbit anti-mouse-CD68 (Abcam,
500 #ab125212), rat anti-mouse-CD41a (invitrogen, #14-0411-82), and rabbit anti-mouse-Fibrinogen
501 (Abcam, #ab34269). Secondary Ab: Alexa Fluor 488 donkey anti-rat-IgG (Invitrogen,
502 #A21208), Alexa Fluor 594 goat anti-rabbit-IgG (Thermo #A11037), Alexa Fluor 546 donkey
503 anti-rabbit-IgG (Invitrogen, #A10040). For quantitative analysis, we selected at least five
504 representative areas that were captured with a Nikon Eclipse E800 fluorescence microscope at a
505 200x magnification. In select experiments, F-actin in neutrophils was stained by rhodamine-
506 conjugated phalloidin (Invitrogen, #R415) for 30 minutes at room temperature following fixation
507 and permeabilization using 0.2% Tween-20.

508 **Statistical analysis**

509 All results are reported as the mean ± SD. Comparison of 2 groups was performed using an
510 unpaired, 2-tailed t-test. Comparison of 3 or more groups was performed by one-way ANOVA,
511 followed by Tukey's post hoc test. Statistical analyses were performed using GraphPad Prism
512 9.0 (GraphPad Software). *P* values less than 0.05 were considered significant.

References

1. M. Vourc'h, A. Roquilly, K. Asehnoune, Trauma-Induced Damage-Associated Molecular Patterns-Mediated Remote Organ Injury and Immunosuppression in the Acutely Ill Patient. *Front. Immunol.* **9**, 1330 (2018).

2. L. D. Lullo, P. B. Reeves, A. Bellasi, C. Ronco, Cardiorenal Syndrome in Acute Kidney Injury. *Seminars in nephrology* **39**, 31–40 (2019).

3. Y. Oishi, I. Manabe, Organ System Crosstalk in Cardiometabolic Disease in the Age of Multimorbidity. *Frontiers Cardiovasc Medicine* **7**, 64 (2020).

4. L. Chen, H. Zhao, A. Alam, E. Mi, S. Eguchi, S. Yao, D. Ma, Postoperative remote lung injury and its impact on surgical outcome. *BMC anesthesiology* **19**, 30–10 (2019).

5. F. F. Hoyer, K. Naxerova, M. J. Schloss, M. Hulsmans, A. V. Nair, P. Dutta, D. M. Calcagno, F. Herisson, A. Anzai, Y. Sun, G. Wojtkiewicz, D. Rohde, V. Frodermann, K. Vandoorne, G. Courties, Y. Iwamoto, C. S. Garris, D. L. Williams, S. Breton, D. Brown, M. Whalen, P. Libby, M. J. Pittet, K. R. King, R. Weissleder, F. K. Swirski, M. Nahrendorf, Tissue-Specific Macrophage Responses to Remote Injury Impact the Outcome of Subsequent Local Immune Challenge. *Immunity* **51**, 899-914.e7 (2019).

6. Y. Ma, T. Zabell, A. Creasy, X. Yang, V. Chatterjee, N. Villalba, E. B. Kistler, M. H. Wu, S. Y. Yuan, Gut Ischemia Reperfusion Injury Induces Lung Inflammation via Mesenteric Lymph-Mediated Neutrophil Activation. *Front. Immunol.* **11**, 586685 (2020).

7. M. D. Okusa, D. L. Rosin, K. J. Tracey, Targeting neural reflex circuits in immunity to treat kidney disease. *Nat Rev Nephrol* **13**, 669–680 (2017).

8. M. Liu, Y. Liang, S. Chigurupati, J. D. Lathia, M. Pletnikov, Z. Sun, M. Crow, C. A. Ross, M. P. Mattson, H. Rabb, Acute kidney injury leads to inflammation and functional changes in the brain. *Journal of the American Society of Nephrology* **19**, 1360–1370 (2008).

9. S. A. Lee, M. Cozzi, E. L. Bush, H. Rabb, Distant Organ Dysfunction in Acute Kidney Injury: A Review. *American journal of kidney diseases : the official journal of the National Kidney Foundation*, doi: 10.1053/j.ajkd.2018.03.028 (2018).

10. Y. Komaru, Y. Z. Bai, D. Kreisel, A. Herrlich, Interorgan communication networks in the kidney–lung axis. *Nat. Rev. Nephrol.* **20**, 120–136 (2024).

11. H. C. Hopps, R. W. Wissler, Uremic pneumonitis. *The American journal of pathology* **31**, 261–273 (1955).

12. R. I. Henkin, M. H. Maxwell, J. F. Murray, Uremic pneumonitis. A clinical, physiological study. *Ann Intern Med* **57**, 1001–8 (1962).

13. K. D. Liu, C. Altmann, G. Smits, C. D. Krawczeski, C. L. Edelstein, P. Devarajan, S. Faubel, Serum interleukin-6 and interleukin-8 are early biomarkers of acute kidney injury and predict prolonged mechanical ventilation in children undergoing cardiac surgery: a case-control study. *Critical care (London, England)* **13**, R104 (2009).

14. F. Z. Khamissi, L. Ning, E. Kefaloyianni, H. Dun, A. Arthanarisami, A. Keller, J. J. Atkinson, W. Li, B. Wong, S. Dietmann, K. Lavine, D. Kreisel, A. Herrlich, Identification of kidney injury released circulating osteopontin as causal agent of respiratory failure. *Sci Adv* **8** (2022).

15. T. Victoni, F. R. Coelho, A. L. Soares, A. de Freitas, T. Secher, R. Guabiraba, F. Erard, R. M. de Oliveira-Filho, B. B. Vargaftig, G. Lauvaux, M. A. Kamal, B. Ryffel, R. Moser, W. Tavares-de-Lima, Local and remote tissue injury upon intestinal ischemia and reperfusion depends on the TLR/MyD88 signaling pathway. *Méd. Microbiol. Immunol.* **199**, 35–42 (2010).

16. Y. Yuan, I. Alwis, M. C. L. Wu, Z. Kaplan, K. Ashworth, D. Bark, A. Pham, J. Mcfadyen, S. M. Schoenwaelder, E. C. Josefsson, B. T. Kile, S. P. Jackson, Neutrophil macroaggregates promote widespread pulmonary thrombosis after gut ischemia. *Sci. Transl. Med.* **9** (2017).

17. Y. Hao, S. Hao, E. Andersen-Nissen, W. M. Mauck, S. Zheng, A. Butler, M. J. Lee, A. J. Wilk, C. Darby, M. Zager, P. Hoffman, M. Stoeckius, E. Papalexi, E. P. Mimitou, J. Jain, A. Srivastava, T. Stuart, L. M. Fleming, B. Yeung, A. J. Rogers, J. M. McElrath, C. A. Blish, R. Gottardo, P. Smibert, R. Satija, Integrated analysis of multimodal single-cell data. *Cell* **184**, 3573-3587.e29 (2021).

18. I. Angelidis, L. M. Simon, I. E. Fernandez, M. Strunz, C. H. Mayr, F. R. Greiffo, G. Tsitsiridis, M. Ansari, E. Graf, T.-M. Strom, M. Nagendran, T. Desai, O. Eickelberg, M. Mann, F. J. Theis, H. B. Schiller, An atlas of the aging lung mapped by single cell transcriptomics and deep tissue proteomics. *Nat Commun* **10**, 963 (2019).

19. J. C. Schupp, T. S. Adams, C. C. Jr., M. S. B. Raredon, Y. Yuan, N. Omote, S. Poli, M. Chioccioli, K.-A. Rose, E. P. Manning, M. Sauler, G. DeIuliis, F. Ahangari, N. Neumark, A. C. Habermann, A. J. Gutierrez, L. T. Bui, R. Lafyatis, R. W. Pierce, K. B. Meyer, M. C. Nawijn, S. A. Teichmann, N. E. Banovich, J. A. Kropski, L. E. Niklason, D. Pe'er, X. Yan, R. J. Homer, I. O. Rosas, N. Kaminski, Integrated Single Cell Atlas of Endothelial Cells of the Human Lung. *Circulation* **144**, 286–302 (2021).

20. V. A. Morikis, S. I. Simon, Neutrophil Mechanosignaling Promotes Integrin Engagement With Endothelial Cells and Motility Within Inflamed Vessels. *Front Immunol* **9**, 2774 (2018).

21. T. Németh, M. Sperandio, A. Mócsai, Neutrophils as emerging therapeutic targets. *Nat. Rev. Drug Discov.* **19**, 253–275 (2020).

22. J. H. Spahn, W. Li, A. C. Bribriesco, J. Liu, H. Shen, A. Ibricevic, J.-H. Pan, B. H. Zinselmeyer, S. L. Brody, D. R. Goldstein, A. S. Krupnick, A. E. Gelman, M. J. Miller, D. Kreisel, DAP12 Expression in Lung Macrophages Mediates Ischemia/Reperfusion Injury by Promoting Neutrophil Extravasation. *J Immunol* **194**, 4039–4048 (2015).

23. K. Ley, C. Laudanna, M. I. Cybulsky, S. Nourshargh, Getting to the site of inflammation: the leukocyte adhesion cascade updated. *Nat. Rev. Immunol.* **7**, 678–689 (2007).

24. A. Hidalgo, E. R. Chilvers, C. Summers, L. Koenderman, The Neutrophil Life Cycle. *Trends Immunol.* **40**, 584–597 (2019).

25. D. M. Redenbach, D. English, J. C. Hogg, The nature of leukocyte shape changes in the pulmonary capillaries. *Am. J. Physiol.-Lung Cell. Mol. Physiol.* **273**, L733–L740 (1997).

26. A. T. Skoutelis, V. Kaleridis, G. M. Athanassiou, K. I. Kokkinis, Y. F. Missirlis, H. P. Bassaris, Neutrophil deformability in patients with sepsis, septic shock, and adult respiratory distress syndrome. *Crit. care Med.* **28**, 2355–9 (2000).

27. H. Saito, J. Lai, R. Rogers, C. M. Doerschuk, Mechanical properties of rat bone marrow and circulating neutrophils and their responses to inflammatory mediators. *Blood* **99**, 2207–2213 (2002).

28. K. Ley, H. M. Hoffman, P. Kubes, M. A. Cassatella, A. Zychlinsky, C. C. Hedrick, S. D. Catz, Neutrophils: New insights and open questions. *Sci Immunol* **3** (2018).

29. M. Mack, J. Cihak, C. Simonis, B. Luckow, A. E. I. Proudfoot, J. Plachý, H. Brühl, M. Frink, H.-J. Anders, V. Vielhauer, J. Pfirstinger, M. Stangassinger, D. Schlöndorff, Expression and Characterization of the Chemokine Receptors CCR2 and CCR5 in Mice. *J Immunol* **166**, 4697–4704 (2001).

30. B. Wang, B. H. Zinselmeyer, H. A. Runnels, T. P. LaBranche, P. A. Morton, D. Kreisel, M. Mack, C. Nickerson-Nutter, P. M. Allen, M. J. Miller, In vivo imaging implicates CCR2+ monocytes as regulators of neutrophil recruitment during arthritis. *Cell. Immunol.* **278**, 103–112 (2012).

31. R. N. Hanna, L. M. Carlin, H. G. Hubbeling, D. Nackiewicz, A. M. Green, J. A. Punt, F. Geissmann, C. C. Hedrick, The transcription factor NR4A1 (Nur77) controls bone marrow differentiation and the survival of Ly6C− monocytes. *Nat. Immunol.* **12**, 778–785 (2011).

32. B. G. Yipp, J. H. Kim, R. Lima, L. D. Zbytnuik, B. Petri, N. Swanlund, M. Ho, V. G. Szeto, T. Tak, L. Koenderman, P. Pickkers, A. T. J. Tool, T. W. Kuijpers, T. K. van den Berg, M. R. Looney, M. F. Krummel, P. Kubes, The lung is a host defense niche for immediate neutrophil-mediated vascular protection. *Sci. Immunol.* **2** (2017).

33. L. Brown, B. G. Yipp, Neutrophil swarming: Is a good offense the best defense? *iScience* **26**, 107655 (2023).

34. E. K. S. Lee, M. R. Gillrie, L. Li, J. W. Arnason, J. H. Kim, L. Babes, Y. Lou, A. Sanati-Nezhad, S. K. Kyei, M. M. Kelly, C. H. Mody, M. Ho, B. G. Yipp, Leukotriene B4-Mediated Neutrophil Recruitment Causes Pulmonary Capillaritis during Lethal Fungal Sepsis. *Cell Host Microbe* **23**, 121-133.e4 (2018).

35. G. S. Worthen, B. S. III, E. L. Elson, G. P. Downey, Mechanics of Stimulated Neutrophils: Cell Stiffening Induces Retention in Capillaries. *Science* **245**, 183–186 (1989).

36. C. Summers, N. R. Singh, J. F. White, I. M. Mackenzie, A. Johnston, C. Solanki, K. K. Balan, A. M. Peters, E. R. Chilvers, Pulmonary retention of primed neutrophils: a novel protective host response, which is impaired in the acute respiratory distress syndrome. *Thorax* **69**, 623 (2014).

37. M. Nishino, H. Tanaka, H. Ogura, Y. Inoue, T. Koh, K. Fujita, H. Sugimoto, Serial Changes in Leukocyte Deformability and Whole Blood Rheology in Patients With Sepsis or Trauma. *J. Trauma: Inj., Infect., Crit. Care* **59**, 1425–1431 (2005).

38. P. Preira, J.-M. Forel, P. Robert, P. Nègre, M. Biarnes-Pelicot, F. Xeridat, P. Bongrand, L. Papazian, O. Theodoly, The leukocyte-stiffening property of plasma in early acute respiratory distress syndrome (ARDS) revealed by a microfluidic single-cell study: the role of cytokines and protection with antibodies. *Crit. Care* **20**, 8 (2016).

39. G. B. Nash, B. Christopher, A. J. Morris, J. A. Dormandy, Changes in the flow properties of white blood cells after acute myocardial infarction. *Br. Hear. J.* **62**, 329 (1989).

40. M. Morikawa, Y. Inoue, Y. Sumi, Y. Kuroda, H. Tanaka, Leukocyte deformability in sepsis-induced DIC. *Acute Med. Surg.* **2**, 13–20 (2015).

41. E. M. Drost, G. Kassabian, H. J. Meiselman, D. Gelmont, T. C. Fisher, Increased Rigidity and Priming of Polymorphonuclear Leukocytes in Sepsis. *Am. J. Respir. Crit. Care Med.* **159**, 1696–1702 (1999).

42. J. Wong, B. Johnston, S. S. Lee, D. C. Bullard, C. W. Smith, A. L. Beaudet, P. Kubes, A minimal role for selectins in the recruitment of leukocytes into the inflamed liver microvasculature. *J. Clin. Investig.* **99**, 2782–2790 (1997).

43. J. P. Mizgerd, B. B. Meek, G. J. Kutkoski, D. C. Bullard, A. L. Beaudet, C. M. Doerschuk, Selectins and neutrophil traffic: margination and Streptococcus pneumoniae-induced emigration in murine lungs. *J. Exp. Med.* **184**, 639–645 (1996).

44. N. Ahuja, A. A. Hernando, C. Altmann, R. Bhargava, J. Bacalja, R. G. Webb, Z. He, C. L. Edelstein, S. Faubel, Circulating IL-6 mediates lung injury via CXCL1 production after acute kidney injury in mice. *American journal of physiology Renal physiology* **303**, F864-72 (2012).

45. D. Kreisel, R. G. Nava, W. Li, B. H. Zinselmeyer, B. Wang, J. Lai, R. Pless, A. E. Gelman, A. S. Krupnick, M. J. Miller, In vivo two-photon imaging reveals monocyte-dependent neutrophil extravasation during pulmonary inflammation. *Proc. Natl. Acad. Sci.***107**, 18073–18078 (2010).

46. H.-M. Hsiao, R. Fernandez, S. Tanaka, W. Li, J. H. Spahn, S. Chiu, M. Akbarpour, D. Ruiz-Perez, Q. Wu, C. Turam, D. Scozzi, T. Takahashi, H. P. Luehmann, V. Puri, G. R. S. Budinger, A. S. Krupnick, A. V. Misharin, K. J. Lavine, Y. Liu, A. E. Gelman, A. Bharat, D. Kreisel, Spleen-derived classical monocytes mediate lung ischemia-reperfusion injury through IL-1β. *The Journal of clinical investigation* **128**, 2833–2847 (2018).

47. H. M. Shepherd, J. M. Gauthier, Y. Terada, W. Li, A. S. Krupnick, A. E. Gelman, D. Kreisel, Updated Views on Neutrophil Responses in Ischemia–Reperfusion Injury. *Transplantation* **106**, 2314–2324 (2022).

48. D. G. Gibson, Haemodynamic factors in the development of acute pulmonary oedema in renal failure. *Lancet Lond Engl* **2**, 1217–20 (1966).

49. E. C. Rackow, I. A. Fein, C. Sprung, R. S. Grodman, Uremic pulmonary edema. *Am J Medicine* **64**, 1084–1088 (1978).

50. C. Laterza, S. Wattananit, N. Uoshima, R. Ge, R. Pekny, D. Tornero, E. Monni, O. Lindvall, Z. Kokaia, Monocyte depletion early after stroke promotes neurogenesis from endogenous neural stem cells in adult brain. *Exp. Neurol.* **297**, 129–137 (2017).

51. S. Choudhary, R. Satija, Comparison and evaluation of statistical error models for scRNA-seq. *Genome Biol.* **23**, 27 (2022).

52. I. Korsunsky, N. Millard, J. Fan, K. Slowikowski, F. Zhang, K. Wei, Y. Baglaenko, M. Brenner, P. Loh, S. Raychaudhuri, Fast, sensitive and accurate integration of single-cell data with Harmony. *Nat. Methods* **16**, 1289–1296 (2019).

53. Y. Kirita, H. Wu, K. Uchimura, P. C. Wilson, B. D. Humphreys, Cell profiling of mouse acute kidney injury reveals conserved cellular responses to injury. *P Natl Acad Sci USA* **117**, 15874–15883 (2020).

54. Y. Zhou, B. Zhou, L. Pache, M. Chang, A. H. Khodabakhshi, O. Tanaseichuk, C. Benner, S. K. Chanda, Metascape provides a biologist-oriented resource for the analysis of systems-level datasets. *Nat. Commun.* **10**, 1523 (2019).

55. H. Wu, R. G. Villalobos, X. Yao, D. Reilly, T. Chen, M. Rankin, E. Myshkin, M. D. Breyer, B. D. Humphreys, Mapping the single-cell transcriptomic response of murine diabetic kidney disease to therapies. *Cell Metab.* **34**, 1064-1078.e6 (2022).

56. X. Qiu, Q. Mao, Y. Tang, L. Wang, R. Chawla, H. A. Pliner, C. Trapnell, Reversed graph embedding resolves complex single-cell trajectories. *Nat. Methods* **14**, 979–982 (2017).

57. S. Jin, C. F. Guerrero-Juarez, L. Zhang, I. Chang, R. Ramos, C.-H. Kuan, P. Myung, M. V. Plikus, Q. Nie, Inference and analysis of cell-cell communication using CellChat. *Nat Commun* **12**, 1088 (2021).

513 **Acknowledgments**

514 Anti-CCR2 antibody used for the *in vivo* monocyte depletion experiment was a generous gift
515 from Prof. Dr. Matthias Mack (Universität Regensburg, Germany). The CCR2-GFP mice were
516 provided by Prof. Dr. Steven Brody (Washington University in St. Louis). We appreciate Prof.
517 Drs. Daniel Kreisel, Kory Lavine, and Regina Clemens (all at Washington University in St.
518 Louis) for useful advice from their expertise. We acknowledge the In vivo Imaging Core (IVIC),
519 at the Washington University School of Medicine, for two-photon imaging and multi-
520 dimensional data analysis.

521 **Funding:**
522 YK was supported by the Japan Society for the Promotion of Science (JSPS) Overseas Research
523 Fellowship (#202360162) and The Uehara Memorial Foundation Overseas Research Fellowship
524 (#202140023). EK was supported by the American Heart Association (Career Development
525 Award 20CDA35320006) and the American Society of Nephrology (KidneyCure Carl W.
526 Gottschalk Research Scholar Grant). MM was supported by National Institute of Allergy and
527 Infectious Diseases (R01AI077600). AH was supported by National Institute of Diabetes and
528 Digestive and Kidney diseases (R01DK121200) and VA merit award (I01BX005322).

529 **Author contributions:**
530 AH conceived and designed the study. YK, LN, CL, and AS performed experiments. YK and
531 MM performed the intra-vital imaging experiment. YK and AH analyzed and interpreted the
532 data, prepared the figures, and wrote the manuscript. AH and MM provided experimental
533 resources. AH supervised the entire project. All authors read and approved the final version of
534 the manuscript.

535 **Competing interests:** Authors declare that they have no competing interests.

536 **Data and materials availability:** Single-cell RNA-seq datasets have been deposited in the Gene
537 Expression Omnibus (GEO) with accession number GSE249928. All data needed to evaluate the
538 conclusions in the paper are available in the main text or Supplementary materials.

539 **Supplementary Materials:**
540 **Fig. S1.** Anti-LFA1 neutralizing antibody did not prevent neutrophil accumulation in the lung
541 after AKI; **Fig. S2.** F-actin staining of the circulating neutrophils 24 hours after sham or AKI;
542 **Movies S1-2.** Intravital two-photon imaging of the lung 2 hours after sham (S1) or AKI (S2).